J. Biochem. 2009;145(5)555–563
doi:10.1093/jb/mvp014

Two Crystal Structures of Lysyl-tRNA Synthetase from *Bacillus stearothermophilus* in Complex with Lysyladenylate-Like Compounds: Insights into the Irreversible Formation of the Enzyme-Bound Adenylate of L-Lysine Hydroxamate

Haruko Sakurama[1], Teisuke Takita[1,*], Bunzo Mikami[2], Takafumi Itoh[2], Kiyoshi Yasukawa[1] and Kuniyo Inouye[1]

[1]Division of Food Science and Biotechnology, Graduate School of Agriculture, Kyoto University, Sakyo-ku, Kyoto 606-8502; and [2]Division of Applied Life Science, Graduate School of Agriculture, Kyoto University, Gokasho, Uji, Kyoto 611-0011, Japan

Received December 9, 2008; accepted December 15, 2008; published online January 27, 2009

Aminoacyl-tRNA synthetase forms an enzyme-bound intermediate, aminoacyladenylate in the amino-acid activation reaction. This reaction is monitored by measuring the ATP-PPi exchange reason in which [^{32}P]PPi is incorporated into ATP. We previously reported that L-lysine hydroxamate completely inhibited the L-lysine-dependent ATP-PPi exchange reaction catalysed by lysyl-tRNA synthetase from *Bacillus stearothermophilus* (*Bs*LysRS). Several experiments suggested that *Bs*LysRS can adenylate L-lysine hydroxamate, but the enzyme-bound lysyladenylate-like compound does not undergo the nucleophilic attack of PPi. This contrasts with the two reports for seryl-tRNA synthetase (SerRS): (i) L-serine hydroxamate was utilized by yeast SerRS as a substrate in the ATP-PPi exchange; and (ii) a seryladenylate-like compound was formed from L-serine hydroxamate in the crystal structure of *Thermus thermophilus* SerRS. To gain clues about the mechanistic difference, we have determined the crystal structures of two complexes of *Bs*LysRS with the adenylate of L-lysine hydroxamate and with 5′-*O*-[*N*-(L-Lysyl)sulphamoyl] adenosine. The comparisons of the two *Bs*LysRS structures and the above SerRS structure revealed the specific side-chain shift of Glu411 of *Bs*LysRS in the complex with the adenylate of L-lysine hydroxamate. In support of other structural comparisons, the result suggested that Glu411 plays a key role in the arrangement of PPi for the nucleophilic attack.

Key words: aminoacyl-tRNA synthetase, crystal structure, L-lysine hydroxamate, lysyl-tRNA synthetase, seryl-tRNA synthetase.

Abbreviations: aaRS, aminoacyl-tRNA synthetase; *Bs*LysRS, lysyl-tRNA synthetase from *Bacillus stearothermophilus*; *Ec*LysRS, LysRS from *Escherichia coli*; Lys, L-lysine; LysSA, 5(-*O*-[*N*-(L-Lysyl) sulphamoyl] adenosine; LXT and LXT-AMP, L-lysine hydroxamate and the adenylate respectively; SXT and SXT-AMP, L-serine hydroxamate and the adenylate, respectively; *Tt*SerRS, seryl-tRNA synthetase from *Thermus thermophilus*.

Aminoacyl-tRNA synthetase (aaRS) catalyses the ligation of the specific amino acid to its cognate tRNA (*1*, *2*).

$$\text{aaRS} + \text{AA} + \text{ATP} \leftrightarrow \text{aaRS} \cdot \text{AA} \sim \text{AMP} + \text{PPi} \quad (1)$$

$$\text{aaRS} \cdot \text{AA} + \text{tRNA} \leftrightarrow \text{aaRS} + \text{AMP} + \text{AA} - \text{tRNA} \quad (2)$$

where AA denotes the amino acid; PPi, inorganic pyrophosphate; AA∼AMP, aminoacyladenylate; and AA-tRNA, aminoacyl-tRNA. The first step is called the amino-acid activation reaction, while the second step is done with the aminoacyl transfer reaction. In most cases, the amino-acid activation reaction is monitored by measuring the highly reversible ATP-PPi exchange reaction in which [^{32}P] PPi is easily incorporated into ATP. In general, all known organisms have 20 aaRSs, each of which corresponding to one of common 20 amino acids. Based on sequence similarity and catalytic domain architecture, aaRSs are classified into two groups, class I and class II. Consistent with this classification, the class I and II aaRSs attach the specific amino acid to the 2′- and 3′-hydroxyl group of the terminal adenosine of the cognate tRNA, respectively (*3*).

Lysyl-tRNA synthetase from *Bacillus stearothermophilus* (*Bs*LysRS) [EC 6.1.1.6] is a homodimer consisting of 493 amino acid residues in each subunit and belongs to the class II. Based on the crystal structures of LysRS from *Escherichia coli* (*Ec*LysRS) (*4*, *5*), it is considered that the subunit consists of an N-terminal anticodon-binding domain (Ser1-Pro144), a C-terminal catalytic domain (Asp152-Lys493) and a polypeptide connecting these two domains (Glu145-Leu151). We have studied the mechanism of the L-lysine (Lys) activation reaction catalysed by *Bs*LysRS (*6–9*). We revealed that the Trp314 is responsible for the fluorescence changes accompanied

*To whom correspondence should be addressed. Tel: +81 75 753 6268, Fax: +81 75 753 6265, E-mail: takita@kais.kyoto-u.ac.jp

© The Authors 2009. Published by Oxford University Press on behalf of the Japanese Biochemical Society. All rights reserved.

Downloaded from http://jb.oxfordjournals.org/ at Islamic Azad University on September 28, 2012

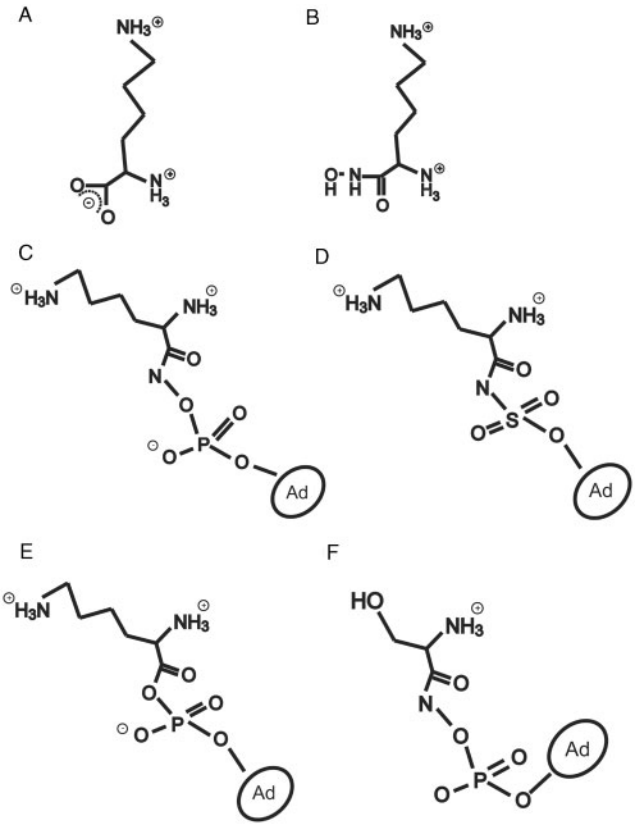

Fig. 1. **Structures of L-lysine and L-serine derivatives.** (A) Lys. (B) LXT. (C) LXT-AMP. (D) LysSA. (E) Lys∼AMP. (F) SXT-AMP. 'Ad' represents adenosine.

with the Lys activation (*10*). We also demonstrated that the activity of its catalytic domain alone markedly decreases, but restores to almost the original level by the addition of the anticodon domain (*11*).

Previously, we reported that L-lysine hydroxamate (LXT) completely inhibited the Lys-dependent ATP-PPi exchange reaction catalysed by *Bs*LysRS due to the formation of the lysyladenylate-like compound (LXT-AMP) and that the enzyme-bound LXT-AMP did not undergo the nucleophilic attack of PPi (*6–8*) (Fig. 1). This is in contrast to the two reports for seryl-tRNA synthetase (SerRS; a class II enzyme). L-serine hydroxamate (SXT) partially, but not completely, inhibited the L-serine-dependent ATP-PPi exchange catalysed by yeast SerRS, and yet the enzyme catalysed the SXT-dependent ATP-PPi exchange (*12*). In the crystal structure of *Thermus thermophilus* SerRS (*Tt*SerRS), a close homologue of yeast SerRS, a seryladenylate-like compound, (SXT-AMP) was formed from SXT (Fig. 1) (*13*). These differences suggest that particular residues of *Bs*LysRS and yeast SerRS play important and distinctive roles in the arrangement of PPi for the nucleophilic attack on the respective enzyme-bound aminoacyladenylates (or the analogues). In this study, in order to identify such residues, we have determined two crystal structures of *Bs*LysRS, one co-crystallized with LXT and ATP and the other co-crystallized with an aminoacylsulphamoyladenosine, 5′-*O*-[*N*-(L-Lysyl)sulphamoyl] adenosine (LysSA) (Fig. 1D). As expected, LXT-AMP and LysSA were contained in their active sites. The structural comparisons of the *Bs*LysRS•LXT-AMP complex, the *Bs*LysRS•LysSA complex, the *Ec*LysRS•Lys∼AMP•PPi complex (*4*), the *Ec*LysRS•Lys•ATP complex (*4*) and the *Tt*SerRS•SXT-AMP omplex (*13*) suggest that the promising candidate is Glu411 of *Bs*LysRS and Glu345 of yeast SerRS.

MATERIALS AND METHODS

Materials—*Bs*LysRS was purified from *E. coli* BL21(DE3) cells harbouring pNB plasmids according to the method described previously (*9*). LXT and ATP were purchased from Sigma (St. Louis, MO, USA). LysSA was from RNA-TEC (Leuven, Belgium). All other chemicals were of reagent grade.

Crystallization—*Bs*LysRS (100 μl of 12 mg/ml) was dialysed at 4°C for 3 days against 200 ml of 50 mM HEPES buffer (pH 7.5) containing 2 mM 2-mercaptoethanol using Slide-A-Lyzer Mini DiaLysis Units 3,500 MWCO (Pierce, Rockford, IL, USA). For the crystallization of the *Bs*LysRS•LXT-AMP complex, the dialysed enzyme (8 mg/ml) was incubated at 37°C for 1 h in a solution of 10 mM LXT, 5 mM $MgCl_2$, 5 mM $MgSO_4$ and 2 mM ATP with the reservoir solution of 0.2 M PIPES buffer (pH 6.8) containing 16% (v/v) polyethylene glycol 4,000 and 1.0 M LiCl. Droplets were prepared by mixing 5 μl of the reaction mixture with 5 μl of a reservoir solution, and were equilibrated against 500 μl of the reservoir solution at 20°C. The crystal was soaked in a cryoprotectant solution of 0.2 M PIPES buffer (pH 6.8) containing 25% (v/v) PEG 400, 10 mM LXT, 5 mM $MgCl_2$, 5 mM $MgSO_4$ and 2 mM ATP for several minutes. For the crystallization of the *Bs*LysRS•LysSA complex, the dialysed enzyme (8 mg/ml) was incubated at 37°C for 1 h in a solution of 4 mM LysSA, 5 mM $MgCl_2$ and 5 mM $MgSO_4$ with the reservoir solution of 0.2 M PIPES buffer (pH 6.8) containing 18% (v/v) polyethylene glycol 4000 and 1.0 M LiCl. Droplets were prepared by mixing 5 μl of the reaction mixture with 5 μl of a reservoir solution, and were equilibrated against 1 ml of the reservoir solution at 20°C. The crystal was soaked in a cryoprotectant solution of 0.2 M PIPES buffer (pH 6.8) containing 25% (v/v) PEG 400, 40 mM LysSA, 5 mM $MgCl_2$ and 5 mM $MgSO_4$ for several minutes. Both crystals were placed in a nitrogen gas stream at 100 K, and stored in liquid nitrogen.

Data Collection—X-ray diffraction images were collected with synchrotron radiation at SPring-8 (Hyogo, Japan). The data collection was carried out at 100 K under a nitrogen gas stream. The images of the *Bs*LysRS•LXT-AMP complex were collected at the beam line BL38B1 using an ADSC Quantum 4R detector at a wavelength of 1.0 Å, while those of the LysSA complex were done at the beam line BL38B1 using a RIGAKU Jupiter 210 detector at a wavelength of 1.0 Å. After processing to resolution of 2.0 Å using the HKL2000 program package (DENZO and SCALEPACK) (*14*), each set of the images ware separately subjected to molecular replacement using the program 'CNS' version 1.1 (*15*). The coordinates of the *Ec*LysRS in the complex with Lys (Protein Data Bank entry code 1BBU) (*5*) with the 2.0 Å

Downloaded from http://jb.oxfordjournals.org/ at Islamic Azad University on September 28, 2012

resolution were used as a model. Since the molecular replacement gave a clear solution, each model was separately refined by simulated annealing with molecular dynamics using a slow-cooling protocol in the program 'CNS'. Several rounds of positional refinement and individual 'B'-factor refinement to 2.2 Å (the *Bs*LysRS•LXT-AMP complex) or 2.0 Å (the *Bs*LysRS•LysSA complex) were carried out using the program CNS. For the calculation of a free 'R' factor, 10% of the reflections were randomly selected and excluded from refinement. Using PRODRG2 (*16*), the topology parameters of LXT-AMP and LysSA were obtained by the energy minimizing of the molecule, which was prepared based on the structures of SXT-AMP or SerSA (*13*). After each cycle of refinement, the model was adjusted manually using the graphics program TURBO-FRODO (AFMB-CNRS, France) on a Silicon Graphics Octane computer. Isolated electron densities >2.7σ in the F_o–F_c map and/or 1.0 σ in the $2F_o$–F_c map were assigned as water molecules when the locations were sterically reasonable. All figures representing LysRS structures were prepared with the programs of MOLSCRIPT (*17*) and RASTER3D (*18*). For the preparation of figures with electron density of the crystal structure, the program of Bobscript (*19*, *20*) was used. The coordinates of the crystal structures have been deposited with the Protein Data Bank as 3EQI for the LXT-AMP complex and 3E9H for the LysSA complex.

RESULTS AND DISCUSSION

Structure Determination—The diffraction data of the *Bs*LysRS•LXT-AMP complex were measured to 2.2 Å resolution, while those of the *Bs*LysRS•LysSA complex were done to 2.1 Å resolution (summarized in Table 1). Both asymmetric units contained two *Bs*LysRS homodimers. The electron densities of the following residues, Ser1-Glu3, Tyr147-Lys151 and Lys493 were much low, and thus their coordinates were not determined.

Figure 2A and B shows the crystal structures of a whole homodimer of the *Bs*LysRS•LXT-AMP complex and that of the *Bs*LysRS•LysSA complex, respectively. Each subunit consists of an N-terminal anticodon-binding domain and a C-terminal catalytic domain with an extended dimmer interface of the catalytic domains. In all active sites (four each for the two complexes), one strong electron density (>3σ) was observed. The electron density in the LXT-AMP complex and that in the LysSA complex were interpreted as LXT-AMP (Fig. 2C) and LysSA (Fig. 2D), respectively. Since one peak density was observed in the proximity of LXT-AMP/LysSA in the respective complexes, it was interpreted as an Mg^{2+} ion. The crystallographic results for the LXT-AMP complex supported our previous proposal that the complete inhibition by LXT of the Lys-dependent ATP-PPi exchange reaction catalysed by *Bs*LysRS is due the irreversible formation of the enzyme-bound LXT-AMP. On the other hand, the result for the LysSA complex is consistent with the report that LysSA is a strong inhibitor of *Ec*LysRS (*21*).

Figure 3 shows the close-up views of the active sites of the two complexes of *Bs*LysRS. In the *Bs*LysRS•LXT-AMP complex (Fig. 3A), the LXT-AMP molecule is located on one side of two anti-parallel β-strands with potential hydrogen bonding to the side chains of the Glu231, Glu255, Glu269, Tyr271 and Glu418. The adenine ring of LXT-AMP is sandwiched between His261 and Phe265. The side chain of Glu411 has two different forms, in which one side chain interacts with an Mg^{2+} ion and the other does with Arg470. The Mg^{2+} ion interacts with the oxygen of the phosphate of LXT-AMP, 3′-hydroxyl group of ribose of LXT-AMP, and the side chains of Glu404 and Glu411. In the *Bs*LysRS•LysSA complex (Fig. 3B), the LysSA molecule is located and recognized in the same manner as the LXT-AMP molecule. However, the Glu411 has a unique form in both of the subunits, in which the side chain interacts with an Mg^{2+} ion, but not with the side chain of Arg470. The Mg^{2+} ion interacts with the oxygen of the sulphamate and the side chains of Glu404 and Glu411. It is remarkable that the position of the Mg^{2+} ion interacting with LXT-AMP is about 3 Å different from the one doing with LysSA.

Structural Comparisons—In order to investigate whether the side-chain shift of Glu411 in the *Bs*LysRS•LXT-AMP complex is specifically caused by the formation of LXT-AMP, we compared the crystal structures of *Bs*LysRS, *Ec*LysRS and *Tt*SeRS. We first compared the *Bs*LysRS•LysSA complex with the *Ec*LysRS•Lys~AMP•PPi complex (*4*). It is considered that the

Table 1. **Data collection and refinement statistics.**

Data collection		
Data set	LXT and ATP	LysSA
X-ray source	BL38B1	BL38B1
Detector	ADSC Quantum 4R	RIGAKU Jupiter210
Space group	$P2_1$	$P2_1$
a (Å), b (Å), c (Å)	79.14, 82.48, 149.78 89.99	79.64, 83.22, 150.82 89.95
Wavelength (Å)	1.000	1.000
Resolution range (Å)	50–2.2 (2.20–2.28)	50–2.05 (2.05–2.12)
Total/unique reflections	298,457/92,075	3,757,661/110,899
Completeness (%)	94.7 (88.9)	89.7 (83.6)
R_{merge} (%)[a]	8.1 (32.0)	8.7 (42.3)
Refinement		
Program used	CNS	CNS
Resolution range (Å)	15–2.2 (2.20–2.28)	15–2.1 (2.10–2.17)
Used reflections	80,851	102,192
Completeness (%)	83.0 (60.8)	89.0 (83.3)
Residues/waters	1,936/498	1,936/463
Average protein B-factor (Å^2)	19.9	25.6
Average waters B-factor (Å ^{2})	17.2	21.7
Bond length r.m.s. (Å)	0.007	0.02
Bond angles r.m.s. (Å)	1.4	2.1
R-factor (%)[b]	18.2 (18.1)	19.1 (25.2)
R_{free}-factor (%)[c]	24.6 (26.9)	24.2 (31.3)

[a] $R_{merge} = \Sigma|I - <I>|/\Sigma <I>$, which I is the observed intensity of reflections. [b] R-factor = Σ $||F_{obs}|-|F_{calc}||/\Sigma$ $|F_{obs}|$. [c] An R_{free}-factor test set of 10% the total reflections was used. Statistics for the highest resolution shell are given in parentheses.

Downloaded from http://jb.oxfordjournals.org/ at Islamic Azad University on September 28, 2012

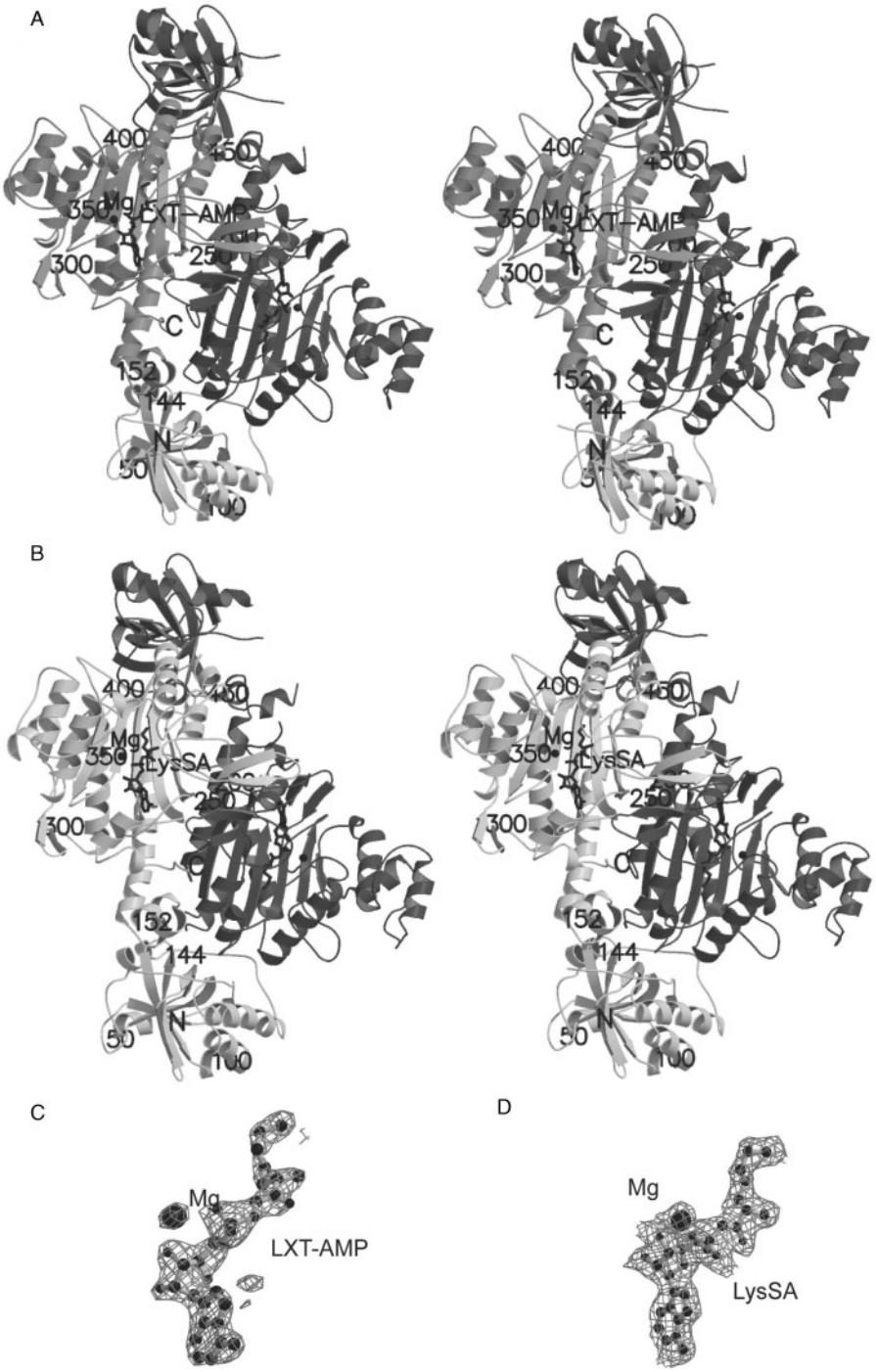

Fig. 2. **The crystal structures of the *Bs*LysRS complexes.** (A) *Bs*LysRS•LXT-AMP. (B) *Bs*LysRS•LysSA. Stereodrowing showing ribbon diagram of the overall structure of the *Bs*LysRS homodimer is shown with the N-terminal anticodon-binding domain (Glu4-Pro144), a C-terminal catalytic domain (Asp152-Lys493). The polypeptide connecting these two domains (Tyr147-Lys151), and Ser1-Glu3 and Lys493 are not shown. The LXT-AMP and LysSA molecules are represented as sticks, and the magnesium ions are done as spheres. 'N' and 'C' indicate the positions of Glu4 and His492, respectively. (C) Fo-Fc map contoured at 2.7 σ showing densities in the active site of *Bs*LysRS corresponding to a LXT-AMP molecule after refinement without LXT-AMP and Mg ion. (D) Fo–Fc map contoured at 2.7 σ showing densities in the active site of BsLysRS corresponding to a LysSA molecule after refinement without LysSA and Mg ion.

active-site structure of the *Bs*LysRS•LysSA complex is very similar to that of the *Bs*LysRS•Lys∼AMP complex. As shown in Fig. 4A, both structures were identical except for a conserved Arg residue, Arg260 in the former and Arg269 in the latter. Figure 4B shows the comparison of the *Bs*LysRS•LXT-AMP complex with the *Ec*LysRS•Lys∼AMP•PPi complex (*4*). In addition to the structural difference for the conserved Arg residue

Downloaded from http://jb.oxfordjournals.org/ at Islamic Azad University on September 28, 2012

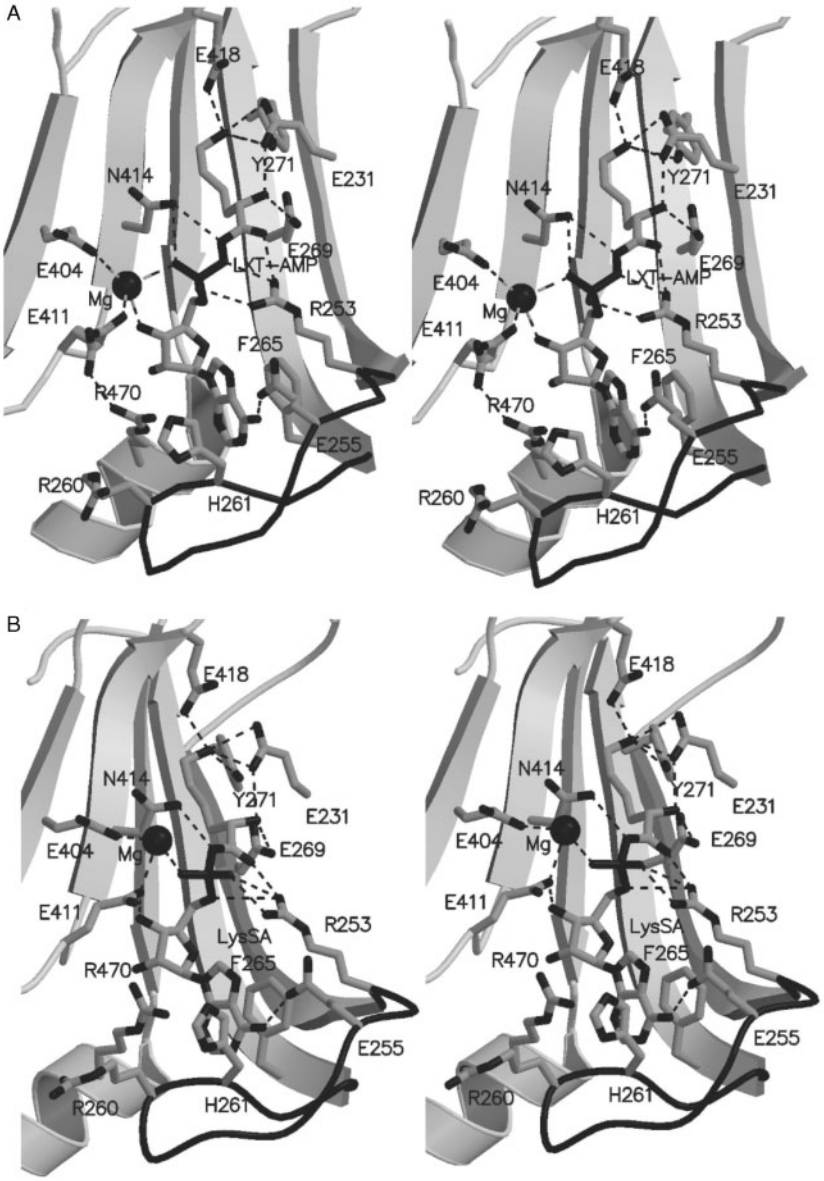

Fig. 3. **Close-up views of the active sites of *Bs*LysRS.** (A) *Bs*LysRS•LXT-AMP. (B) *Bs*LysRS•LysSA. Stereodrowing showing ribbon diagram of the active site of *Bs*LysRS is shown. The side chains of the key residues for the binding of lysyladenylate, LXT-AMP and LysSA are represented as sticks, and the Mg^{2+} ions are as spheres.

(Fig. 4A), significant differences were observed for the following pairs: (i) the α-phosphate moieties of LXT-AMP and Lys∼AMP; (ii) the side-chains of Glu411 of *Bs*LysRS and of Glu421 of *Ec*LysRS; and (iii) the Mg^{2+} ions close to the α-phosphate moieties of LXT-AMP and Lys∼AMP. Further, PPi molecule was not observed in the *Bs*LysRS•LXT-AMP complex in contrast to the *Ec*LysRS•Lys∼AMP•PPi complex. Since the backbone of LXT-AMP is longer by one atom than those of Lys∼AMP and LysSA (Fig. 1), it is considered that the backbone extension results in the side-chain shift of Glu411 in the *Bs*LysRS•LXT-AMP complex. It is considered that the shift of Glu411 is closely associated with the shift of the Mg^{2+} ion, which is induced as a result of the interactions of the Mg^{2+} ion with the oxygen of the phosphate and the 3′-hydroxyl group of ribose of LXT-AMP and with the side chains of Glu404 and Glu411. The position of the Mg^{2+} ion in the *Bs*LysRS• LysSA complex is occupied by the side chain of Glu411 in the *Bs*LysRS•LXT-AMP complex. In the *Ec*LysRS• Lys∼AMP•PPi complex, it seems likely that the PPi molecule is rearranged at a better position for the nucleophilic attack on the phosphorus atom of Lys∼AMP since the space surrounded by Lys∼AMP, Lys, the Mg^{2+} ions, Glu421 and Arg480 is wide enough for the PPi molecule to further move.

Figure 4C shows the comparison of the *Ec*LysRS• Lys•ATP complex with the *Ec*LysRS•Lys∼AMP•PPi complex (*4*). The *Ec*LysRS•Lys•ATP complex was prepared in the presence of Mn^{2+} instead of Mg^{2+} to repress the formation of lysyladenylate. Their active-site structures were almost identical, suggesting that the side-chain shift

Downloaded from http://jb.oxfordjournals.org/ at Islamic Azad University on September 28, 2012

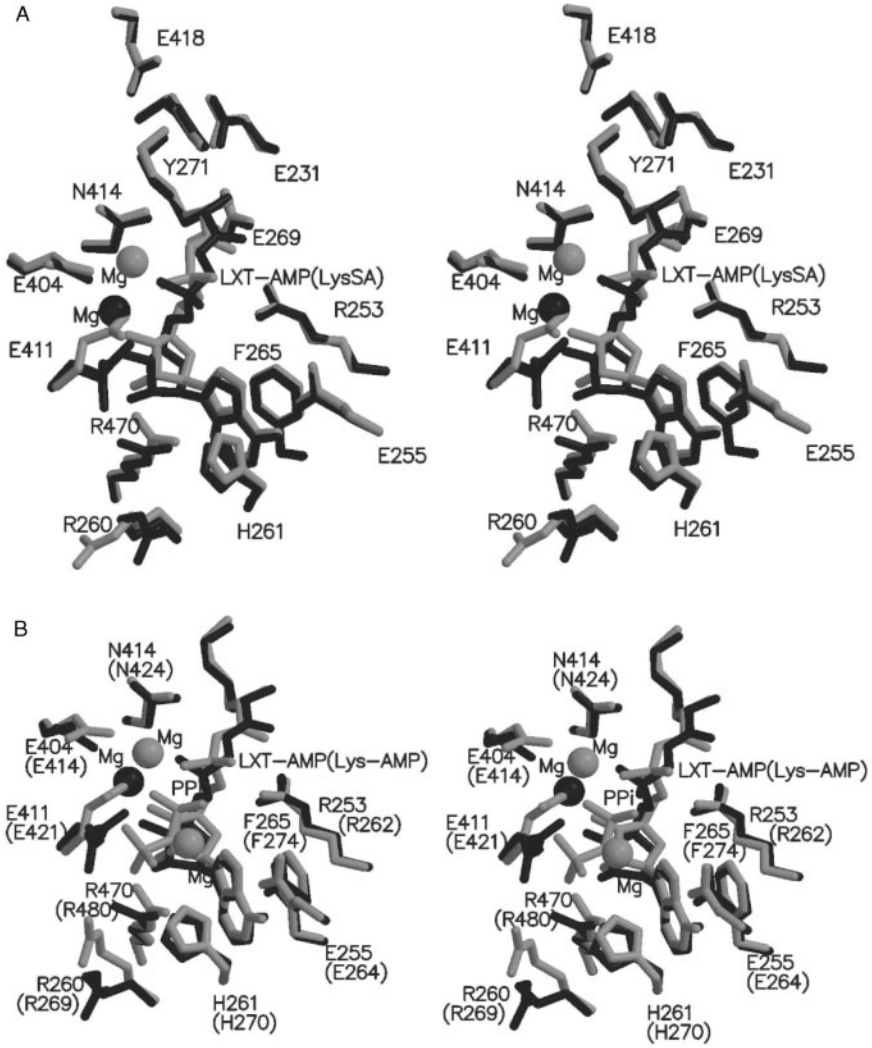

Fig. 4. **Superimposition of the active-site structures.** (A) *Bs*LysRS•LysSA (black) *vs*. *Ec*LysRS•Lys∼AMP•PPi (grey). (B) *Bs*LysRS•LXT-AMP (black) *vs*. *Ec*LysRS•Lys∼AMP•PPi (grey). (C) *Ec*LysRS•Lys∼AMP•PPi. (black) *vs*. *Ec*LysRS•Lys•ATP (grey). (D) *Bs*LysRS•LXT-AMP (black) *vs*. *Ec*LysRS•Lys•ATP (grey). (E) *Bs*LysRS•LXT-AMP (black) *vs*. *Tt*SerRS•SXT-AMP (grey). Streodrowing is shown. The side chain of the key residues for the recognition of the adenylate moiety, LXT-AMP, LysSA, Lys∼AMP, Lys•ATP and PPi are represented as sticks. The Mg^{2+} ions of *Bs*LysRS•LXT-AMP, *Bs*LysRS•LysSA and *Ec*LysRS•Lys∼AMP•PPi and the Mn^{2+} ions of *Ec*LysRS•Lys∼AMP•PPi and *Ec*LysRS•Lys•ATP are represented as spheres. The key residues in parentheses are as follows. (A) *Ec*LysRS•Lys-AMP•PPi. (B) *Ec*LysRS•Lys∼AMP•PPi. (D) *Ec*LysRS•Lys•ATP. (E) *Tt*SerRS•SXT-AMP. The structures of *Ec*LysRS•Lys∼AMP•PPi, *Ec*LysRS•Lys•ATP and *Tt*SerRS•SXT-ATP are derived from Protein Data Bank entry code 1E1T, 1E24, and 1SES, respectively.

of Glu411 of *Bs*LysRS (Glu421 of *Ec*LysRS) does not occur upon the formation of lysyladenylate. Figure 4D shows the comparison of the *Bs*LysRS•LXT-AMP complex with the *Ec*LysRS•Lys•ATP complex (*4*). This comparison emphasized the uniqueness of the side-chain position of Glu411 in the *Bs*LysRS•LXT-AMP complex. Figure 4E shows the comparison of the *Bs*LysRS•LXT-AMP complex with the *Tt*SerRS•SXT-AMP complex (*13*). The Mg^{2+} ion was observed in the former but not in the latter. The side-chain positions of Glu404 and Glu411 of *Bs*LysRS were significantly different from those of Asp332 and Glu345 of *Tt*SerRS, respectively. Although the two active-site structures are much different due to the sequence difference, it seems that the Mg^{2+} ion is not be retained well in the *Tt*SerRS•SXT-AMP complex as compared with the *Bs*LysRS•LXT-AMP complex because Glu404 of *Bs*LysRS is replaced with Asp332 in *Tt*SerRS and yet the side chain of Asp332 makes a hydrogen bond with the side chain of Ser348, which destabilize the possible binding of Mg^{2+} ion. As a result, the side chain of Glu345 in the *Tt*SerRS•SXT-AMP complex is located at the position of the Mg^{2+} ion in *Bs*LysRS•LXT-AMP complex, where Glu411 in the *Bs*LysRS•LysSA complex and Glu421 in the *Ec*LysRS•Lys∼AMP•PPi complex are located (Fig. 4).

Insights into the Irreversible Formation of HXT-ATP by BsLysRS—The structural comparisons described above showed that Glu411 residues in the *Bs*LysRS•LXT-AMP

Downloaded from http://jb.oxfordjournals.org/ at Islamic Azad University on September 28, 2012

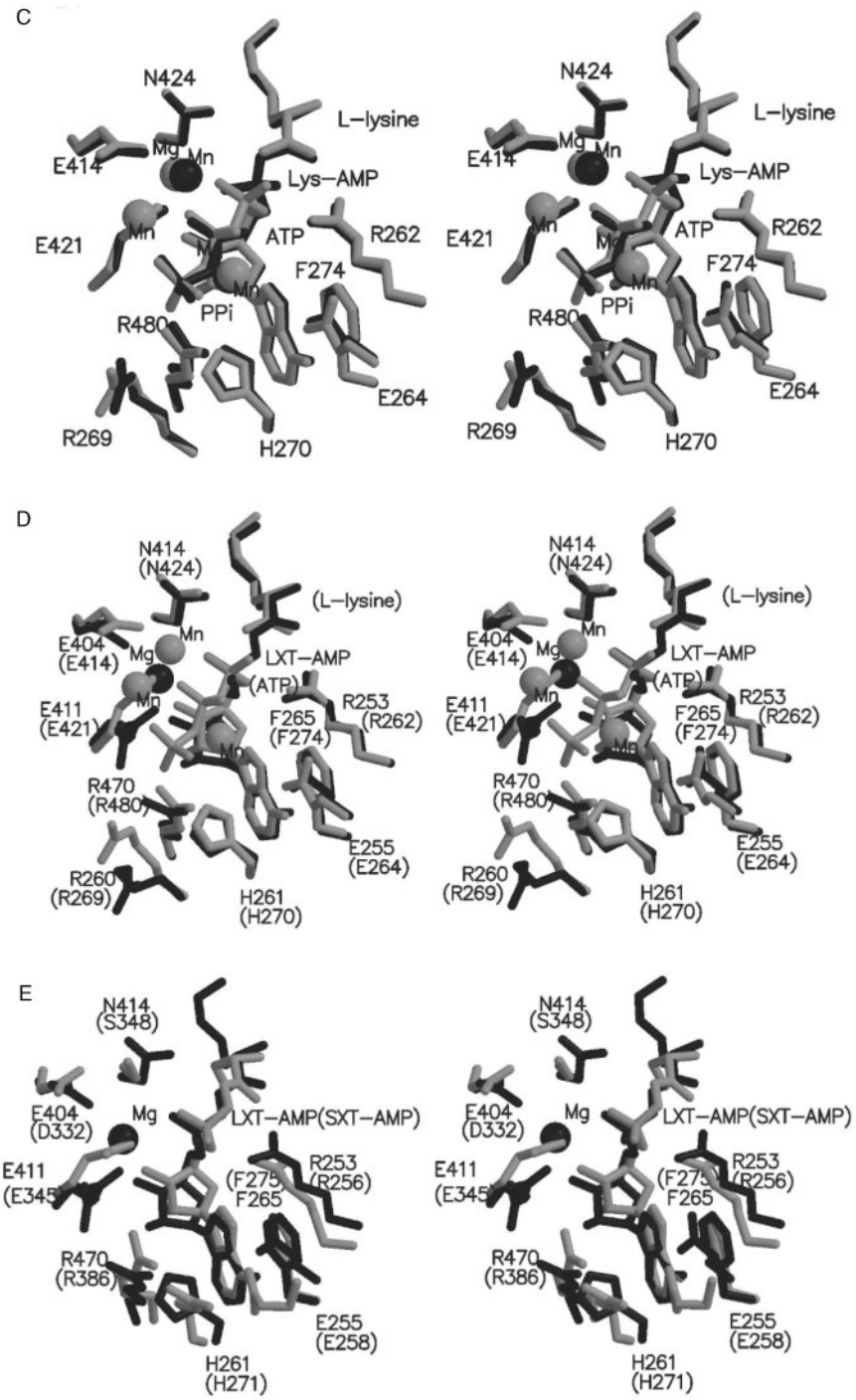

Fig. 4. Continued.

complex have two forms and occupy unique positions, which are not occupied by the counterparts in the other four complexes (Fig. 4). In addition, the side chain of Glu411 in the LXT-AMP complex is shifted towards the adenine ring, compared to those of the counterparts in the four complexes. For example, the distances from the N9 atom of the adenine ring to the CG atom of the conserved Glu residue in the respective complexes are as follows: 6.1–6.3 Å in the *Bs*LysRS•LXT-AMP (Fig. 3A); 7.1 Å in the *Bs*LysRS•LysSA (Fig. 3B); 7.2 Å in the *Ec*LysRS•Lys~AMP•PPi (Fig. 4B); and 7.3 Å in the *Tt*SerRS•SXT-AMP (Fig. 4E). We consider that the *ca.* 1 Å side-chain shift of Glu411 in the LXT-AMP complex is key to understanding the following mechanistic difference: *Bs*LysRS-bound LXT-AMP does not undergo the nucleophilic attack of PPi, whereas yeast SerRS-bound SXT-AMP undergoes it. The non-occurrence of the attack of PPi on the LXT-AMP is explained as

Downloaded from http://jb.oxfordjournals.org/ at Islamic Azad University on September 28, 2012

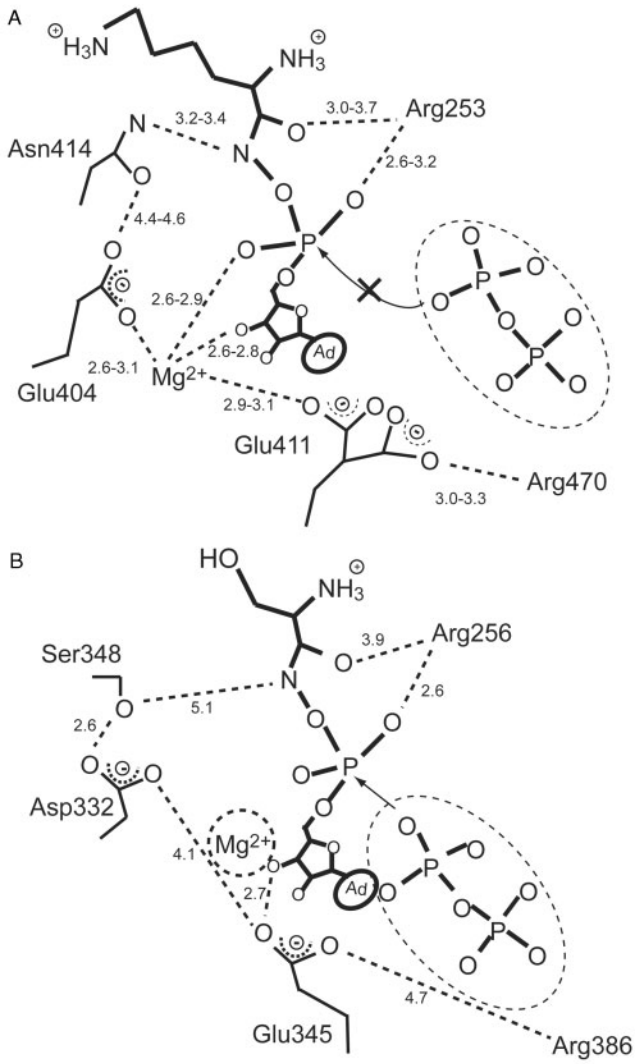

Fig. 5. **Schematic representation of a mechanism in which the nucleophilic attack of PPi on the LXT-AMP does not occur**. (A) *Bs*LysRS•LXT-AMP. Glu411 blocks the PPi binding. (B) *Tt*SerRS•SXT-AMP. Glu345 does not block the PPi binding. Distances between atoms are indicated in angstrom. 'Ad' represents adenine. The positions of the PPi molecules (A and B) and the Mg^{2+} ion (B) were determined by the calculation.

follows (Fig. 5A). After the LXT-AMP formation, the Mg^{2+} ion is shifted towards Glu411 and the side-chain of Glu411 slides towards the adenine ring, giving the two forms of Glu411. Both of them block the binding of PPi to the LXT-AMP complex or make impossible the arrangements of PPi that permit its nucleophilic attack on the enzyme-bound LXT-ATP. The reduced PPi-binding capacity of the LysRS•LXT-AMP complex, compared with that of the LysRS•Lys∼AMP complex, is supported by the crystallographic results, the non-existence of PPi in the *Bs*LysRS•LXT-AMP complex and the existence in the *Ec*LysRS•Lys∼AMP•PPi complex (Fig. 4B). On the other hand, details of the occurrence of the nucleophilic attack of PPi on the yeast SerRS-bound SXT-AMP are uncertain because the Mg^{2+}-binding (position) has not been confirmed in any SerRS structures. However, it seems to be reasonable to postulate that an Mg^{2+} is arranged in and around the putative Mg^{2+}-binding site of yeast SerRS upon the attack of PPi on the SXT-AMP because it would be crucial to the stabilization of the transition state of the α-phosphate. As described above, it is considered that the Mg^{2+}-binding affinity of *Tt*SerRS is reduced as compared with that of *Bs*LysRS, due to the replacement of Glu404 of *Bs*LysRS with Asp332 of *Tt*SerRS and the formation of the hydrogen bond between the Asp332 and Ser348 in *Tt*SerRS (Fig. 5B). The potential residues of *Tt*SerRS involved in the Mg^{2+} binding (Asp332, Glu345 and Ser348) are all conserved in yeast SerRS (Asp353, Glu366 and Ser369, respectively). Thus, SXT binds yeast SerRS, but the resulting shift of the Mg^{2+} ion and Glu366 (Glu345 in *Tt*SerRS) are limited. Therefore, the side chains of Glu345 in the *Tt*SerRS•SXT-AMP complex and Glu366 in the yeast SerRS•SXT-AMP complex exist at the position of the shifted Mg^{2+} ion of the *Bs*LysRS•LXT-AMP complex and they are thought not to block the PPi binding (Fig. 5B).

Inhibitors of aaRSs—Because aaRS is an essential enzyme for protein biosynthesis, its inhibitors might be clinically useful as antibacterial agent (*22*). Mupirocin, a natural antibiotic produced by *Pseudomonas fluorescence*, inhibits bacterial isoleucyl-tRNA synthetase and is clinically used to control infections by methicillin-resistant *Staphylococcus aureus* (MRSA) (*22*, *23*). On the other hand, aminoacylsulphamoyladenosines and aminoalkyl adenylates have been synthesized and evaluated for their inhibitory activities on aaRSs. Hydroxamate-linked and aminoacyladenylate-like compounds, such as LXT-AMP and SXT-AMP, have not been noticed as the inhibitors of aaRSs. We previously demonstrated that LXT completely inhibits the *Bs*LysRS activity in the Lys-dependent ATP-PPi exchange reaction with the inhibitor constant, K_i, value of $0.6 \pm 0.2\,\mu M$ (*6*, *7*). It was reported that in the amino -acid activation reaction by *Es*LysRS, the K_i values of LXT and LysSA were $86 \pm 7\,\mu M$ and $0.028 \pm 0.003\,\mu M$, respectively (*21*). This might give the impression that LXT is not an effective inhibitor. However, the K_i value of LXT is comparable to other inhibitors such as L-lysine amide, L-lysine methyl ester and L-lysine ethyl ester (*21*). In this study, we suggested that Glu411 of *Bs*LysRS plays a key role in the irreversible formation of LXT-AMP. Further structural study is required to evaluate LXT-AMP or other hydroxamate-linked and aminoacyladenylate-like compounds as clinically useful inhibitors of bacterial aaRSs.

FUNDING

Grants-in-Aid for Scientific Research (10760049, 12760055 and 15770084 to T.T., partial) from the Japan Society of the Promotion of Sciences.

CONFLICT OF INTEREST

None declared.

Downloaded from http://jb.oxfordjournals.org/ at Islamic Azad University on September 28, 2012

REFERENCES

1. Berg, P. (1961) Specialty in protein synthesis. *Annu. Rev. Biochem.* **30**, 293–322
2. Fersht, A.R. and Kaethner, M.M. (1976) Mechanism of aminoacylation of tRNA. Proof of the aminocyl adenylate pathway for the isoleucyl- and tyrosyl- tRNA synthetase form *Escherichia coli* K12. *Biochemistry* **15**, 818–823
3. Eriani, G., Delarue, M., Poch, O., Gangloff, J., and Moras, D. (1990) Partition of tRNA syntheases into two classes based on mutually exclusive sets of sequence motifs. *Nature* **347**, 203–206
4. Desogus, G., Todone, F., Brick, P., and Onesti, S. (2000) Active site of lysyl-tRNA synthetase: structural studies of the adenylation reaction. *Biochemistry* **39**, 8418–8425
5. Onesti, S., Desogus, G., Brevet, A., Chen, J., Plateau, P., Blanquet, S., and Brick, P. (2000) Structural studies of lysyl-tRNA synthetase: conformational changes induced by substrate binding. *Biochemistry* **39**, 12853–12861
6. Takita, T., Ohkubo, Y., Shima, H., Muto, T., Shimizu, N., Sukata, T., Ito, H., Saito, Y., Inouye, K., Hiromi, K., and Tonomura, B. (1996) Lysyl-tRNA synthetase from *Bacillus stearothermophilus*. Purification, and fluorometric and kinetic analysis of the binding of substrates, L-lysine and ATP. *J. Biochem.* **119**, 680–689
7. Takita, T., Hashimoto, S., Ohkubo, Y., Muto, T., Shimizu, N., Sukata, T., Inouye, K., Hiromi, K., and Tonomura, B. (1997) Lysyl-tRNA synthetase from *Bacillus stearothermophilus*. Formation and isolation of the enzyme•lysyladenylate complex and its analogue. *J. Biochem.* **121**, 244–250
8. Takita, T., Akita, E., Inouye, K., and Tonomura, B. (1998) Lysyl-tRNA synthetase fro m *Bacillus stearothermophilus*. Stopped-flow kinetic anaLysis of enzyme•lysyladenylate formation. *J. Biochem.* **124**, 45–50
9. Takita, T., Shimizu, N., Sukata, T., Hashimoto, S., Akita, E., Yokota, Y., Esaki, N., Soda, K., Inouye, K., and Tonomura, B. (2000) Lysyl-tRNA synthetase from *Bacillus stearothermophilus*. Molecular cloning and expression of the gene. *Biosci. Biotechnol. Biochem.* **64**, 432–437
10. Takita, T., Nakagoshi, M., Inouye, K., and Tonomura, B. (2003) Lysyl-tRNA synthetase from *Bacillus stearothermophilus*: the Trp314 residue is shielded in a non-polar environment and is responsible for the fluorescence changes observed in the amino acid activation reaction. *J. Mol. Biol.* **325**, 677–695
11. Takita, T. and Inouye, K. (2002) Transition state stabilization by the N-terminal anticodon-binding domain of lysyl-tRNA synthetase. *J. Biol. Chem.* **277**, 29275–29282
12. Landeka, I., Filipic-Rocak, S., Zinic, B., and Weygand-Durasevic, I. (2000) Characterization of yeast seryl-tRNA synthetase active site mutants with improved discrimination against substrate analogues. *Biochim. Biophys. Acta* **1480**, 160–170
13. Belrhali, H., Yaremchuk, A., Tukalo, M., Larsen, K., Berthet-Colominas, C., Leberman, R., Beijer, B., Sproat, B., Als-Nielsen, J., Grübel, G., Legrand, J.-F., Lehmann, M., and Cusack, S. (1994) Crystal structures at 2.5 angstrom resolution of seryl-tRNA synthetase complexed with two analogs of seryl adenylate. *Science* **263**, 1432–1436
14. Otwinowski, Z. and Minor, W. (1997) Processing of X-ray diffraction data collected in oscillation mode. *Methods Enzymol.* **276**, 307–326
15. Brünger, A.T., Adams, P.D., Clore, G.M., DeLano, W.L., Gros, P., Grosse-Kunstleve, R.W., Jiang, J.S., Kuszewski, J., Nilges, M., Pannu, N.S., Read, R.J., Rice, L.M., Simmon, T., and Warren, G.L. (1998) Crystallography and NMR system (CNS): a new software system for macromolecular structure determination. *Acta Crystallogr. Sect. D* **54**, 905–921
16. Schüettelkopf, A.W. and van Aalten, D.M.F. (2004) PRODRG - a tool for high-throughput crystallography of protein-ligand complexes. *Acta Crystallogr. Sect. D* **60**, 1355–1363
17. Kraulis, P.J. (1991) MOLSCRIPT: a program to produce both detailed and schematic plots of protein structure. *J. Appl. Crystallogr.* **24**, 946–950
18. Merrit, E.A. and Murphy, M.E.P. (1994) Raster3D Version 2.0. A program for photorealistic molecular graphics. *Acta Crystallogr. Sect. D.* **50**, 869–873
19. Esnouf, R.M. (1997) An extensively modified version of MolScript that includes greatly enhanced coloring capabilities. *J. Mol. Graph. Model.* **15**, 132–134
20. Esnouf, R.M. (1997) An extensively modified version of MolScript that includes greatly enhanced coloring capabilities. *J. Mol. Graph. Model.* **15**, 112–113
21. Levengood, J., Ataide, S.F., Roy, H., and Ibba, M. (2004) Divergence in noncognate amino acid recognition between class I and class II lysyl-tRNA synthetases. *J. Biol. Chem.* **279**, 17707–17714
22. Berneir, S., Akochy, P.-M., Lapointe, J., and Chenevert, R. (2005) Synthesis and aminoacyl-tRNA synthetase inhibitory activity of aspartyl adenylate analogues. *Bioorg. Med. Chem.* **13**, 69–75
23. Fuller, A.T., Mellows, G., Woolford, M., Banks, G.T., Barrow, K.D., and Chain, E.B. (1971) Pseudomonas acid: an antibiotic produced by *Pseudomonas fluorescens*. *Nature* **234**, 416–417

Downloaded from http://jb.oxfordjournals.org/ at Islamic Azad University on September 28, 2012